

# Improved measurements of the foreign-broadened continuum of water vapor in the 6.3 $\mu\text{m}$ band at $-30\text{ }^\circ\text{C}$

Penny M. Rowe<sup>1</sup> and Von P. Walden<sup>1</sup>

<sup>1</sup> *Department of Geography, University of Idaho, Moscow, Idaho 83843, USA*

*\* Corresponding author: [prowe@harbornet.com](mailto:prowe@harbornet.com)*

Atmospheric emission in the  $\nu_2$  band of water vapor by the foreign-broadened continuum (1300-2000  $\text{cm}^{-1}$ ) is important for retrievals of upper tropospheric water vapor. Previous work reported continuum coefficients retrieved from two downwelling emission measurements made with the Polar Atmospheric Emitted Radiance Interferometer (PAERI) at temperatures characteristic of the upper troposphere (below  $-25\text{ }^\circ\text{C}$ ) at Dome C, Antarctica. These results are improved upon using 19 additional measurements. Improvements have been made to the PAERI radiance calibration, the radiance simulations, and the error analysis. Compared to the Mlawer, Tobin, Clough, Kneizys, Davies continuum, the retrieved continuum is found to be 20 to 50% lower from 1350 to 1490  $\text{cm}^{-1}$  and 0 to 20% higher from 1850 to 1980  $\text{cm}^{-1}$ .

*OCIS codes: 010.1280, 28.4991, 300.6340.*

## 1. Introduction

Water vapor is the most effective greenhouse gas on Earth, and, therefore, accurate water-vapor absorption coefficients are important for determining the Earth's radiation budget. Accurate absorption coefficients are also needed for retrieving tropospheric humidity from satellite-based

measurements of infrared radiation. Retrievals of upper tropospheric humidity typically make use of the  $\nu_2$  band of water vapor (1300 to 2000  $\text{cm}^{-1}$ ; 5 to 7.7  $\mu\text{m}$ ). For example, this region is used to retrieve water vapor and other trace gas amounts from the Atmospheric Infrared Sounder (AIRS) on the Earth Observing System (EOS) Aqua spacecraft [1]. An important part of the absorption coefficient is the continuum between strong lines of water vapor. The upper troposphere is characterized by temperatures between -25 and -80  $^{\circ}\text{C}$ , and is dry enough that line broadening by non-water molecules (foreign broadening) is more important than self-broadening by water molecules. It is therefore important to have accurate measurements of the foreign-broadened continuum of water vapor in the  $\nu_2$  band at low temperatures.

Recent theoretical calculations of the far wing lineshape of the self-broadened continuum from 300 to 1100  $\text{cm}^{-1}$  [2] agree fairly well with laboratory measurements. Moreover, the temperature dependence is predicted down to 250 K. However, within the  $\nu_2$  band it is difficult to theoretically predict the magnitude of the continuum and thus its temperature dependence. Contributions from the far-wings are a minor contribution to the total continuum in-band, and theoretical calculations of collision-induced broadening show that it is about an order of magnitude too small to explain the continuum [3]. Therefore, it is believed that non-Lorentzian absorption coefficients in the near-wing are important [2]. At the present time, continuum models must rely on measurements of the continuum within the  $\nu_2$  band rather than theoretical calculations. When predictions of the temperature dependence of the foreign-broadened continuum coefficient in the band do become available, it will be important to have accurate experimental results to compare them to.

Continuum coefficients in the  $\nu_2$  band have been measured both in the laboratory and in field experiments. Laboratory measurements are typically performed at close to room

temperature (over long absorption paths; e.g. [4]), while field measurements are typically made from atmospheres with effective temperatures that are much warmer than the upper troposphere [5-7]. Many such measurements have been used to develop the widely-used empirical model of Mlawer, Tobin, Clough, Kneizys and Davies (MT-CKD, [8]). Based on past measurements, this continuum model assumes no temperature dependence for foreign-broadening.

In previous work by the authors [9] foreign-broadened continuum coefficients of water vapor from 1300 to 2000  $\text{cm}^{-1}$  were retrieved at effective temperatures near  $-30\text{ }^{\circ}\text{C}$ . Continuum coefficients were retrieved by comparing measurements of downwelling atmospheric emission to radiance simulations. The emission measurements were made by the Polar Atmospheric Emitted Radiance Interferometer (PAERI) under clear skies during two austral summer field seasons at Dome C, Antarctica: during the afternoon on 15 January 2003 and during the late evening on 12 December 2003. (The experiment was performed in support of ground-based validation of the AIRS [10-12].) In addition to the PAERI measurements, atmospheric temperature, pressure, and humidity were measured during the Dome C experiment with Vaisala RS80 and RS90 radiosondes [13,14]. These atmospheric profiles were used to simulate downwelling radiances. Comparisons of the simulated radiances to measured radiances were used to retrieve the continuum coefficients, and the continuum coefficients were then compared to the MT-CKD continuum.

Since the previous work, nineteen additional clear-sky datasets have been identified during December 2003 and January 2004. Vaisala RS90 radiosoundings coincide with all datasets. Temperature and water vapor profiles have been corrected by Rowe et al. [14] using updated lineshape parameters (HITRAN; [15]) and improved retrieval techniques. Furthermore, improvements have been made to the emissivity function of the infrared sources used to calibrate

the measured radiances [16], as well as in the lineshape parameters affecting the simulated radiances. Several sources of error have been reduced and the calibration uncertainty, an important source of error, has been included. These improvements result in retrieved continuum coefficients that are more accurate and have better-characterized uncertainties.

In this work, we describe the various improvements and then compare the water-vapor continuum coefficients retrieved for the additional measurements to the previous results. Because this work provides supplemental results to those previously published, we focus on what is novel in this work, referencing the previous work [9] as RWW06. The datasets used in this work have been discussed in detail in [14].

The continuum is given here as a cross section in units of  $\text{cm}^2 \text{ molecule}^{-1}$ , given by the symbol  $C_f$ , as in RWW06.  $C_f$  is related to the absorption coefficient  $k$  according to

$$k = C_f \left( \frac{\rho_f}{\rho_o} \right) + C_s \left( \frac{\rho_s}{\rho_o} \right) + k_{local},$$

where  $\rho_f$  and  $\rho_s$  are the densities of air and water vapor and  $\rho_o$  is a reference density at standard temperature and pressure,  $C_s$  is the self-broadened continuum, and  $k_{local}$  is defined as the sum of the peaks of strong lines, or the “local” part of the Lorentz line shape [6,9].

## 2. Instrumentation

### *a. Vaisala RS90 Radiosondes*

Atmospheric temperature, pressure, and humidity were measured in clear skies using 19 Vaisala RS90 radiosondes. The Vaisala series of radiosondes are described elsewhere in detail (e.g. [13,

17, 18]). The particular radiosondes used in this field project are described by Rowe et al. [14]. Radiosonde temperature profiles have been corrected using comparisons of the measured radiances with modeled radiances [14]. The correction procedure benefits from improvements in the HITRAN database to the CO<sub>2</sub> lineshape parameters from 700 to 780 cm<sup>-1</sup> [15]. The Vaisala RS90 radiosonde humidities have been corrected for the time lag of the sensor [19] and for dry biases due to calibration error and solar heating of the humidity sensor [14].

### *b. The Polar Atmospheric Emitted Radiance Interferometer (PAERI)*

The PAERI is a ground-based infrared spectrometer developed by the Space Science and Engineering Center (SSEC) at the University of Wisconsin, Madison; the interferometer was manufactured by BOMEM. It is described in detail by Knuteson et al. [20, 21]. The PAERI has two detectors; the channel 1 detector is sensitive from 500 to 1800 cm<sup>-1</sup> and the channel 2 detector is sensitive from 1750 to 3000 cm<sup>-1</sup>. The PAERI measurements used here are described by RWW06 and Rowe et al. [14]. Radiances are calibrated to very high accuracy using measurements of emission from two blackbodies, one at ambient temperature and one at 40 °C. The emissivity of the blackbodies has been carefully characterized [22], including recent improvement to the emissivity model. This improvement accounts for a change in the radiance of about 0.1 mW m<sup>-2</sup> sr<sup>-1</sup> (cm<sup>-1</sup>)<sup>-1</sup> at 961 cm<sup>-1</sup> (1 mW m<sup>-2</sup> sr<sup>-1</sup> (cm<sup>-1</sup>)<sup>-1</sup> = 1 RU) and 0.02 RU at 1350 cm<sup>-1</sup>. The effect of this improvement on the retrieval of the continuum coefficients is discussed in Section 4 below. Figure 1 shows the PAERI measurement made on 13 January 2004 from 0730 to 0830 UT in the  $\nu_2$  band. (A PAERI “measurement” is actually the average of several spectral measurements made during the duration of the sounding. These individual spectra, in turn, are averages of up to 90 co-additions.)

Improvements were made in determining the uncertainty in the PAERI measurements due to uncertainties in the detector nonlinearity correction, the calibration, and the effective laser wavenumber (ELW). In addition to these, instrument noise is an important source of uncertainty. Knuteson et al. [21] describe the uncertainty due to the nonlinear response of the detector to signal. After correcting for detector nonlinearity, they state that the uncertainty remaining is 2% of 10% of the radiance of the ambient-temperature blackbody. However, this source of error is difficult to quantify and seems likely to be an overestimation. Thus this value is now assumed to be the 3-sigma uncertainty, whereas it was previously assumed to be the 1-sigma uncertainty. The reduction in uncertainty is approximately offset by including the uncertainty in the radiance calibration, which was omitted in RWW06 but is included in both [14] and in this work. Uncertainty in the effective laser wavenumber (ELW) and instrument noise are discussed in both RWW06 and in reference [14]. Since the ELW is sensitive to small changes in the detector position, the ELWs were expected to differ for the two PAERI measurements used in RWW06, as they were made during different field seasons. Thus, the ELW was determined for each dataset and used to assign wavenumbers to each corresponding set of radiances. In this work, by contrast, all 19 datasets should have the same ELW. Thus, the average of the ELWs determined for each dataset was used to assign wavenumbers to the radiances for all datasets, reducing the uncertainty. In addition, the effective laser wavenumber for the channel 2 detector was determined using a revised method that resulted in lower residuals near strong line centers. The individual contributions to the uncertainty in the PAERI measurements in the  $\nu_2$  band are shown in Fig. 2. The noise equivalent spectral radiance (NESR) varies depending on the number of sky-view measurements averaged; figure 2 shows the mean for the 19 datasets. The total uncertainty is approximately equal to the NESR from

1300 to 1900  $\text{cm}^{-1}$ , while from 1900 to 2000  $\text{cm}^{-1}$ , the total uncertainty is only about 0.006 RU, because the channel 2 detector has very low noise. Expressed as a percentage of the measured radiance, the total uncertainty in this spectral region is typically between 1 and 10%.

### 3. Inferring Continuum Coefficients

#### *a. Simulated Radiances*

Radiances were simulated using the line-by-line radiative transfer model (LBLRTM; [23]). In RWW06, version 7.1 was used; version 10.3 is used here. Differences between the two model versions do not affect the retrieved continuum coefficients. However, the differences in the lineshape parameters that were used are important; the HITRAN 2004 database [15] is used here rather than HITRAN 2000 (with updates from 2001; [24]) as in RWW06. In HITRAN 2004, carbon dioxide lineshape parameters have been updated, resulting in improved agreement between measured and simulated radiances between 670 and 720  $\text{cm}^{-1}$ . Because these frequencies are used to correct the temperature profile, the temperature correction is now more accurate, and the uncertainties in the temperature profile are reduced from 0.5 K (RWW06) to 0.13 K [14]. The uncertainties in the water-vapor lineshape parameters listed in the HITRAN database have been reduced in the 2004 version, but those uncertainties were not used previously. In RWW06, uncertainties in the water-vapor lineshape parameters in HITRAN 2000 were found to be unrealistically high and therefore more reasonable estimates were used (see RWW06 and references therein). These estimates are similar to the uncertainties given in the HITRAN 2004 database [15] and that are used here.

In RWW06, a water-vapor scaling factor was determined to correct a dry bias in the Vaisala RS80 and RS90 radiosonde humidities by comparing measured and simulated radiances

near strong line centers from 1100 to 1300  $\text{cm}^{-1}$ . The water-vapor scale factors used in this work are those determined in [14] for the RS90 radiosonde, using both the spectral region from 1100 to 1300  $\text{cm}^{-1}$  and an independent set of frequencies in micro-windows between strong water vapor lines from 530 to 560  $\text{cm}^{-1}$ . Using both sets of frequencies is advantageous because the primary sources of error differ for each set: at strong line centers near 1200  $\text{cm}^{-1}$ , uncertainties in water-vapor lineshape parameters dominate, and in micro-windows near 550  $\text{cm}^{-1}$ , uncertainties in the continuum dominate (the continuum coefficients near 550  $\text{cm}^{-1}$  are not retrieved in this work; for details on the continuum in this spectral region see [6,14]. The uncertainties in the water-vapor amounts are 5% in RWW06 and 4 to 5% for this work (based on [14]).

### *b. Inferring the Continuum Coefficients*

To infer continuum coefficients, forward calculations of simulated radiances were made using the MT-CKD continuum as input to LBLRTM. For each frequency, a multiplier to the continuum was varied until the simulated radiance agreed with the measured radiance; the multiplier resulting in agreement then determined the continuum coefficient. The continuum coefficient was allowed to vary between a factor of -5 and 100. Although by definition the continuum must be positive, negative results were allowed to prevent biasing the mean results high; means were determined in bins of 5 to 10 wavenumbers. Spectral data points were excluded where the simulated radiance was not sufficiently sensitive to emission from the water vapor continuum to retrieve continuum coefficients.

### *c. Uncertainty Analysis*

Sources of error in both the measured and simulated radiances contribute to uncertainty in the retrieved continuum. Each source of uncertainty in the radiance is propagated to an uncertainty in the continuum according to

$$\sigma_c^2 = \left(\frac{\partial C}{\partial I_M}\right)^2 \left(\frac{\partial I_M}{\partial x}\right)^2 \sigma_x^2 + \dots + \left(\frac{\partial C}{\partial I_s}\right)^2 \left(\frac{\partial I_s}{\partial y}\right)^2 \sigma_y^2 + \dots,$$

where  $I_M$  and  $I_s$  are the measured and simulated radiances and  $x$  and  $y$  are corresponding uncertainties from various sources. Each frequency-dependent term is calculated numerically and classified as random-with-frequency or correlated-with-frequency. As equations 3 through 6 in RWW06 show, uncertainties that are random with frequency are reduced by averaging nearby points, while uncertainties that are correlated with frequency become better defined, but are not reduced. Similarly, uncertainties that are random with measurement are reduced by averaging results from the 19 measurements. Thus, these errors are significantly reduced in this study relative to RWW06, where only two measurements were used.

For measured radiances, noise is random with frequency, and the uncertainty in the effective laser wavenumber is treated as random with frequency because it varies rapidly with wavenumber. Both are random with measurement. Detector nonlinearity and calibration uncertainty are correlated with both frequency and measurement. For simulated radiances, uncertainties in the temperature profile, water-vapor amount, and concentrations of CH<sub>4</sub> and N<sub>2</sub>O are correlated with frequency but are treated as random with measurement (although bias errors are possible). Errors in lineshape parameters may be random with frequency within a bin, but to be conservative we treat them as correlated both with frequency and measurement. Sources of error in both the measured radiances and the simulated radiances are discussed in detail by [14].

#### *d. Averaging Continuum Coefficients*

The continuum coefficients retrieved from the 19 PAERI measurements can be averaged to reduce random errors. The coefficients at neighboring frequencies can also be averaged, since the continuum is assumed to vary smoothly with frequency. To average continuum coefficients at neighboring frequencies, we use the same method as RWW06. The frequency range for each detector is first divided into bins of 5 to 10 wavenumbers, containing 20 or fewer data points. For each measurement, data points are chosen in each bin that result in the lowest weighted-mean error. Figure 3 demonstrates this for the dataset of 13 January 2003 at 0730 UT. Only data points used in determining the weighted mean are shown (dots with narrow error bars); actual measured data points are approximately every  $0.5 \text{ cm}^{-1}$ , but most of these were unsuitable. The weighted mean continuum coefficient is also shown for each bin. To show the relative contributions of systematic and random errors, two sets of error bars are shown at each point; the set encompassing the smaller range includes only systematic error while the set encompassing the larger range includes both systematic and random error.

Figure 4 shows the logarithm of the continuum coefficients from the 19 datasets, after taking the weighted mean of continuum coefficients in bins of 5 to  $10 \text{ cm}^{-1}$ . Binned continuum coefficients are shown for both channels; the two channels overlap from 1750 to  $1800 \text{ cm}^{-1}$ . Below  $1350 \text{ cm}^{-1}$  most of the retrieved continuum coefficients are negative (not shown). It is not clear why the error bars are not large enough in this region; it is possible there is a systematic bias in the concentration of a trace gas, such as  $\text{CH}_4$  or  $\text{N}_2\text{O}$ . Because of this, this region is excluded from the remainder of the results.

After averaging continuum coefficients within spectral bins, we can take the weighted-mean average over the results from the 19 datasets to get a final set of continuum coefficients.

As a check on the error analysis, the standard deviation within each bin was compared to the propagated random error for the weighted means. These two estimates of the random error are independent, since the former depends on the standard deviation between measurements while the latter is calculated independently for each measurement by propagating errors. The two estimates of random error agree to within 60%. It is not expected that they should agree exactly, but it is important that the error budget has not been grossly underestimated. Also, although we have averaged nearby continuum coefficients first and then averaged over measurement, the resulting continuum coefficients are similar if the order of averaging is switched.

#### 4. Results and Discussion

The final set of continuum coefficients ( $C_f$ ) is shown in Fig. 5a. Figure 5b shows the logarithm of  $C_f$ . Both figures also show the smooth curve fit to the continuum coefficients of RWW06. Error bars are shown where the error is larger than the size of the symbol. Error bars near the two peaks are large enough to encompass both the RWW06 continuum and the MT-CKD continuum. From about 1620 to 1680  $\text{cm}^{-1}$ , we cannot infer a temperature dependence in this region, but it is interesting that these results agree very well with the previous continuum even though points in this spectral region were not reported from the PAERI in RWW06, but rather with a different instrument (an open-path transmissometer). In both wings of the band, the new results appear to be lower than the previous results; in the low-wavenumber wing this means the new results are less similar to MT-CKD than the previous results, while in the high-wavenumber wing the new results are more similar to MT-CKD than previously. This is shown more clearly in the expanded views in Fig. 6a for the low-wavenumber wing and Fig. 6c for the high-wavenumber wing. The center of the band is shown in Fig. 6b. These figures also show the fit to these results, described below. For clarity, error bars are not shown for the previous results in

panels (a) and (c); the error bars are typically similar to those for the present results at similar frequencies. Changes to the blackbody emissivity function have the greatest effect in the wings of the bands, where the downwelling radiance is small. Sensitivity studies suggest that the new blackbody emissivity function results in continuum coefficients that are lower by between 18% and 4% (as percentage of the continuum) from 1300 to 1350  $\text{cm}^{-1}$  and between 5% and 40% from 1900 to 2000  $\text{cm}^{-1}$ . The improved temperature profiles allow continuum coefficients to be retrieved at more frequencies than in RWW06. Error bars are approximately the same as in RWW06 in the wings of the band, where including the calibration uncertainty more than offsets the reductions in other sources of error. Closer to the center of the band, errors are lower in the present work due to reductions in the temperature uncertainty, noise, and other random errors. Perhaps most importantly, meaningful results are retrieved at more frequencies than previously.

To create the fits to the present work, a separate polynomial fit was used in each of the three regions. The smallest degree polynomials were used that gave a good fit to the data while remaining smoothly varying with frequency. For the low and high wavenumber regions (Fig 6a,c), 3<sup>rd</sup> and 4<sup>th</sup> degree polynomials were used. A weighted least squares fit was used so that the fit depends more strongly on points with smaller error bars; such points are typically farther from line center in clearer microwindows. Thus, for example, the two points with large error bars near 1465  $\text{cm}^{-1}$  have little influence on the fit. The results in the middle of the band (Fig. 6b) were difficult to fit to a polynomial in such a way that the curvature was similar to that of MT-CKD near 1580 and 1620  $\text{cm}^{-1}$ , and an 8<sup>th</sup> degree polynomial was needed. In this region, the error bars for the current work are considerably smaller than RWW06, and suggest that the continuum is not as smooth as MT-CKD.

## 5. Conclusions

Continuum coefficients are retrieved from measurements of downwelling atmospheric radiation. The measurements were made by the Polar Atmospheric Emitted Radiance Interferometer (PAERI), at Dome C, Antarctica during the austral summer of 2003/2004. The continuum coefficients represent an improvement upon the results of a previous work (RWW06), based on only two PAERI measurements. In the present work, continuum coefficients are retrieved from 19 PAERI measurements. In addition, improvements have been made to the data and error analyses. Improvements have been made to the blackbody emissivity function used to calibrate the PAERI measurements. Improvements in the HITRAN CO<sub>2</sub> lineshape parameters [15] result in improved temperature retrievals and thus, more accurate simulations. The error budget has been refined; the uncertainty due to detector nonlinearity previously given as one standard deviation is now assumed to be three standard deviations, and calibration uncertainty is included. Finally, the effective laser wavenumber is better characterized.

The continuum coefficients retrieved in this work are compared to the continuum coefficients retrieved in RWW06 and to the MT-CKD continuum model. The revised continuum coefficients are found to be lower than those of RWW06 in the upper and lower wavenumber regions, resulting in a greater difference from MT-CKD from 1350 to 1490 cm<sup>-1</sup>, while from 1830 to 1900 cm<sup>-1</sup> the new results are closer to the MT-CKD continuum. Assuming that the widely used MT-CKD continuum corresponds to temperatures near 296 K, these results suggest that for the range of tropospheric temperatures, the foreign-broadened continuum may have a positive temperature dependence from 1350 to 1490 cm<sup>-1</sup> (where the results at -30 °C are 20 to 50% lower) and a negative temperature dependence from 1850 to 1980 cm<sup>-1</sup> (where the results at -30 °C are 0 to 20% higher). In the center of the band, near 1600 cm<sup>-1</sup>, the error bars suggest that

the continuum is not as smooth as MT-CKD. The continuum coefficients are fit to a polynomial in each of the three regions and the results are summarized in Tables 1-3.

We are grateful to the Global Monitoring Division of the Earth System Research Laboratory [formerly the Climate Monitoring and Diagnostics Laboratory (CMDL)] for making available their measurements of the concentrations of atmospheric trace gases from South Pole Station. Vital logistical support for our fieldwork at Dome C was provided by the Programma Nazionale di Ricerche in Antartide (PNRA), the Institut Polaire Français Paul Emile Victor (IPEV), and the Office of Polar Programs at the National Science Foundation. We thank Karim Agabi (U. Nice), Eric Aristidi (U. Nice), Tony Travouillon (U. New South Wales), Bradley Halter (U. Idaho), and W. Lance Roth (U. Idaho) for launching radiosondes at Dome C, and Halter and Roth for also operating the P-AERI. This project was supported by NASA grant NAG5-11112 and NSF grant 02-30114 from the Office of Polar Programs.

## References

1. M. T. Chahine and coauthors, "AIRS, Improving Weather Forecasting and Providing New Data on Greenhouse Gases." *Bull. Amer. Meteor. Soc.* 911-926 (2006).
2. Q. Ma and R. H. Tipping (2008), "Temperature dependences of mechanisms responsible for the water-vapor continuum absorption. I. Far wings of allowed lines," *J. Chem. Phys.* 128, 124313, DOI: 10.1063/1.2839604.
3. A. Brown and R. H. Tipping, *Weakly Interacting Paris: Unconventional Absorbers of Radiation in the Atmosphere*, edited by C. Camy-Peyret and A. A. Vigasin. (Kluwer Academic, 2003), p. 99.

4. D. C. Tobin, L. L. Strow, W. J. Lafferty, and W. B. Olson, "Experimental investigation of the self- and N<sub>2</sub>-broadened continuum within the  $\nu_2$  band of water vapor," *Appl. Opt.* **35**, 4724-4734 (1996).
5. J. M. Theriault, P. L. Roney, D. St. Germain, H. E. Revercomb, R. O. Knuteson, and W. L. Smith, "Analysis of the FASCODE model and its H<sub>2</sub>O continuum based on long-path atmospheric transmission measurements in the 4.5-11.5  $\mu\text{m}$  region," *Appl. Opt.* **33**, 323-333 (1994).
6. D. C. Tobin and Coauthors, "Downwelling spectral radiance observations at the SHEBA ice station: Water vapor continuum measurements from 17 to 26  $\mu\text{m}$ ," *J. Geophys. Res.* **104**, D2, 2081-2092 (1999).
7. D. D. Turner and Coauthors, "The QME AERI LBLRTM: A closure experiment for downwelling high spectral resolution infrared radiance," *J. Atmos. Sci.* **61**, 2657-2675 (2004).
8. E. J. Mlawer, S. A. Clough, and D. C. Tobin, "The MT\_CKD water vapor continuum: a revised perspective including collision induced effects," presented at the Atmospheric Science from Space using Fourier Transform Spectrometry (ASSFTS) Workshop, Bad Wildbad (Black Forest), Germany 8-20 October 2003.
9. P. M. Rowe, V. P. Walden and S. G. Warren, "Measurements of the foreign-broadened continuum of water vapor in the 6.3-mm band at -30°C," *Appl. Opt.* **45**, 4366-4382 (2006).
10. V. P. Walden, M.S. Town, B. Halter, and J. W. V. Storey, "First measurements of the infrared sky brightness at Dome C, Antarctica," *Publ. Astron. Soc. Pac.* **117** (829), 300-308 (2005).

11. V. P. Walden, W. L. Roth, R. S. Stone, and B. Halter, "Radiometric validation of the Atmospheric Infrared Sounder over the Antarctic Plateau," *J. Geophys. Res.* **111**, D09S03, doi:10.1029/2005JD006357 (2006).
12. A. Gettelman, V. P. Walden, L. M. Miloshevich, W. L. Roth, and B. Halter, "Relative humidity over Antarctica from radiosondes, satellites, and a general circulation model," *J. Geophys. Res.* **111**, D09S13, doi: 10.1029/2005JD006636 (2006).
13. A. Paukkunen, V. Antikainen, and H. Jauhiainen, "Accuracy and performance of the new Vaisala RS90 radiosonde in operational use," presented at the 11<sup>th</sup> AMS Symposium on Meteorological Observations and Instrumentation, Albuquerque, New Mexico, 14-18 January 2001.
14. P. M. Rowe, L. M. Miloshevich, D. D. Turner, and V. P. Walden, "Dry bias in Vaisala RS90 radiosonde humidity profiles over Antarctica," *J. Atmos. Oceanic Technol.*, accepted (2008).
15. L. S. Rothman and Coauthors, "The HITRAN 2004 molecular spectroscopic database," *J. Quant. Spectrosc. Radiat. Transfer* **96**, 139-204 (2005).
16. Dave Turner, Space Science and Engineering Center, University of Wisconsin – Madison, 1225 West Dayton Street, Madison, WI, 53706 (personal communication, 2008).
17. L. M. Miloshevich, H. Vömel, A. Paukkunen, A. J. Heymsfield, and S. J. Oltmans, "Characterization and correction of relative humidity measurements from Vaisala RS80-A radiosondes at cold temperatures," *J. Atmos. Oceanic Technol.* **18**, 135-156 (2001).
18. J. Wang, H. L. Cole, D. J. Carlson, E. R. Miller, K. Beierle, A. Paukkunen and T. K. Laine, "Corrections of Humidity Measurement Errors from the Vaisala RS80 Radiosonde - Application to TOGA COARE Data," *J. Atmos. Oceanic Technol.* **19**, 981-1002 (2002).

19. L. M. Miloshevich, A. Paukkunen, H. Vömel and S. J. Oltmans, “Development and validation of a time-lag correction for Vaisala radiosonde humidity measurements,” *J. Atmos. Oceanic Technol.* **21**, 1305-1327 (2004).
20. R. O. Knuteson and Coauthors, “Atmospheric Emitted Radiance Interferometer (AERI) Part I: Instrument Design,” *J. Atmos. Oceanic Technol.* **21**, 1763-1776 (2004a).
21. R. O. Knuteson and Coauthors, “Atmospheric Emitted Radiance Interferometer (AERI) Part II: Instrument Performance,” *J. Atmos. Oceanic Technol.* **21**, 1777-1789 (2004b).
22. Fred Best, Space Science and Engineering Center, University of Wisconsin – Madison, 1225 West Dayton Street, Madison, WI, 53706 (personal communication, 2003, 2007).
23. S. A. Clough, M. W. Shephard, E. J. Mlawer, J. S. Delamere, M. J. Iacono, K. Cady-Pereira, S. Boukabara, and P. D. Brown, “Atmospheric radiative transfer modeling: a summary of the AER codes. Short communication,” *J. Quant. Spectrosc. Radiat. Transfer* **91**, 233-244 (2005).
24. L. S. Rothman and Coauthors, “The HITRAN molecular spectroscopic database: edition of 2000 including updates of 2001,” *J. Quant. Spectrosc. Radiat. Transfer* **82**, 5-44 (2003).

## List of Figures

Fig. 1. The radiance measured in the  $\nu_2$  band of water vapor by the Polar Atmospheric Infrared Radiance Interferometer (PAERI) at Dome C, Antarctica on 13 January 2004 at 0730 UT. The solid line represents the emission measured by the channel 1 detector, while the dashed line represents that measured by the channel 2 detector; the two overlap from 1750 to 1800  $\text{cm}^{-1}$ .

Fig. 2. Sources of uncertainty in the downwelling radiance measured by the Polar Atmospheric Infrared Radiance Interferometer (PAERI) at Dome C, Antarctica on 13 January 2004 at 0730 UT. Contributions to the uncertainty are the noise equivalent spectral radiance (NESR), and uncertainties in calibration (Calib.), the detector's nonlinear response to signal (DN), and the effective laser wavenumber (ELW).

Fig. 3. Continuum coefficients retrieved on 13 January 2003 at 0730 UT in four bins (vertical dashed lines). Measurements were made approximately every 0.5  $\text{cm}^{-1}$ , but only continuum coefficients that are used in the average are shown (dots with narrow error bars). The error bar encompassing the smaller range is that due only to errors that are correlated with frequency, while the upper-magnitude also includes errors that are random with frequency. The large circles (with wide error bars) indicate the weighted-mean continuum coefficients within each bin. The MT-CKD continuum is shown for reference (dashed line).

Fig. 4. Logarithm of continuum coefficients retrieved from 19 measurements made with the Polar Atmospheric Infrared Radiance Interferometer (PAERI) at Dome C, Antarctica for

channels 1 and 2 (Ch. 1 and Ch. 2). The points show the weighted mean of continuum coefficients in bins of 5 to 10 wavenumbers. The MT-CKD continuum is shown for reference.

Fig. 5. (a) Final set of continuum coefficients retrieved in this work from Polar Atmospheric Infrared Radiance Interferometer (PAERI) measurements for the channel 1 and channel 2 detectors, and (b) the log of the continuum coefficients. Error bars are omitted where they are smaller than the symbol used. The MT-CKD continuum and the smoothed results of previous work (RWW06) are also shown.

Fig. 6. Continuum coefficients retrieved from Polar Atmospheric Infrared Radiance Interferometer (PAERI) measurements in (a) the low-wavenumber wing of the  $\nu_2$  band, (b) the center, and (c) the high-wavenumber wing. The results of previous work (RWW06) and the MT-CKD continuum are shown.

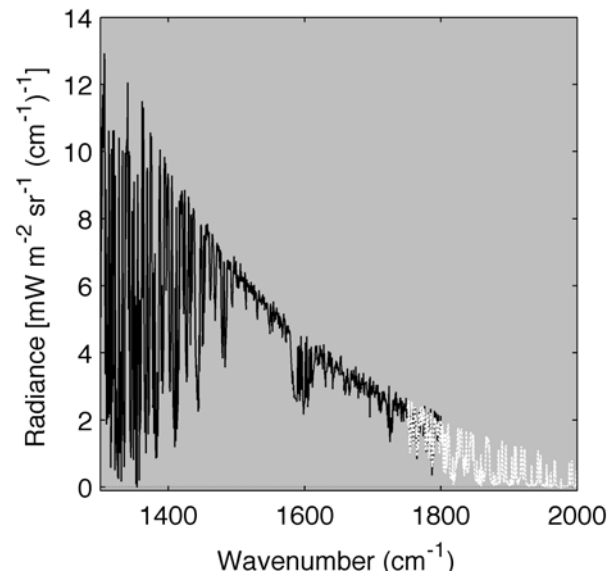


Fig. 1. The radiance measured in the  $\nu_2$  band of water vapor by the Polar Atmospheric Infrared Radiance Interferometer (PAERI) at Dome C, Antarctica on 13 January 2004 at 0730 UT. The solid line represents the emission measured by the channel 1 detector, while the dashed line represents that measured by the channel 2 detector; the two overlap from 1750 to 1800  $\text{cm}^{-1}$ .

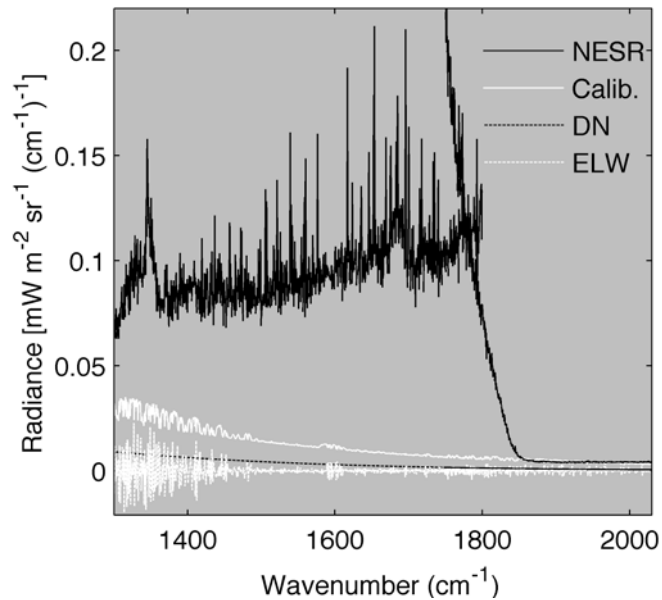


Fig. 2. Sources of uncertainty in the downwelling radiance measured by the Polar Atmospheric Infrared Radiance Interferometer (PAERI) at Dome C, Antarctica on 13 January 2004 at 0730 UT. Contributions to the uncertainty are the noise equivalent spectral radiance (NESR), and uncertainties in calibration (Calib.), the detector's nonlinear response to signal (DN), and the effective laser wavenumber (ELW).

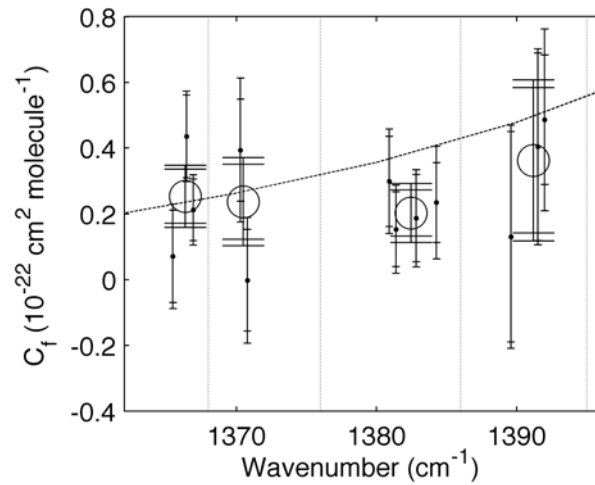


Fig. 3. Continuum coefficients retrieved on 13 January 2003 at 0730 UT in four bins (vertical dashed lines). Measurements were made approximately every  $0.5 \text{ cm}^{-1}$ , but only continuum coefficients that are used in the average are shown (dots with narrow error bars). The error bar encompassing the smaller range is that due only to errors that are correlated with frequency, while the upper-magnitude also includes errors that are random with frequency. The large circles (with wide error bars) indicate the weighted-mean continuum coefficients within each bin. The MT-CKD continuum is shown for reference (dashed line).

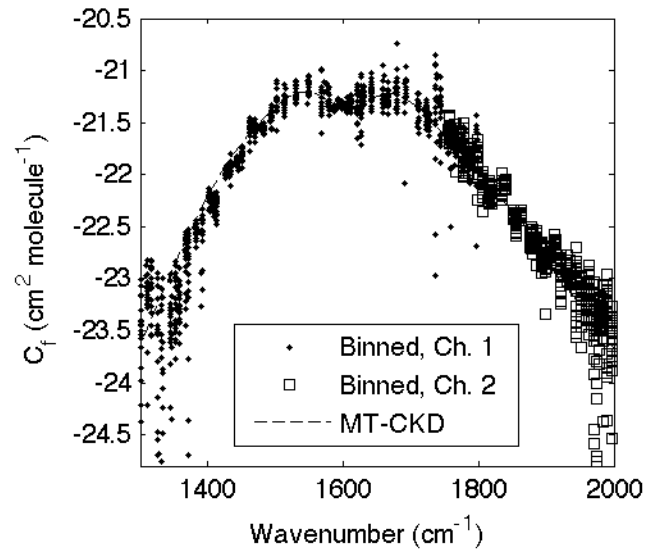


Fig. 4. Logarithm of continuum coefficients retrieved from 19 measurements made with the Polar Atmospheric Infrared Radiance Interferometer (PAERI) at Dome C, Antarctica for channels 1 and 2 (Ch. 1 and Ch. 2). The points show the weighted mean of continuum coefficients in bins of 5 to 10 cm<sup>-1</sup>. The MT-CKD continuum is shown for reference.

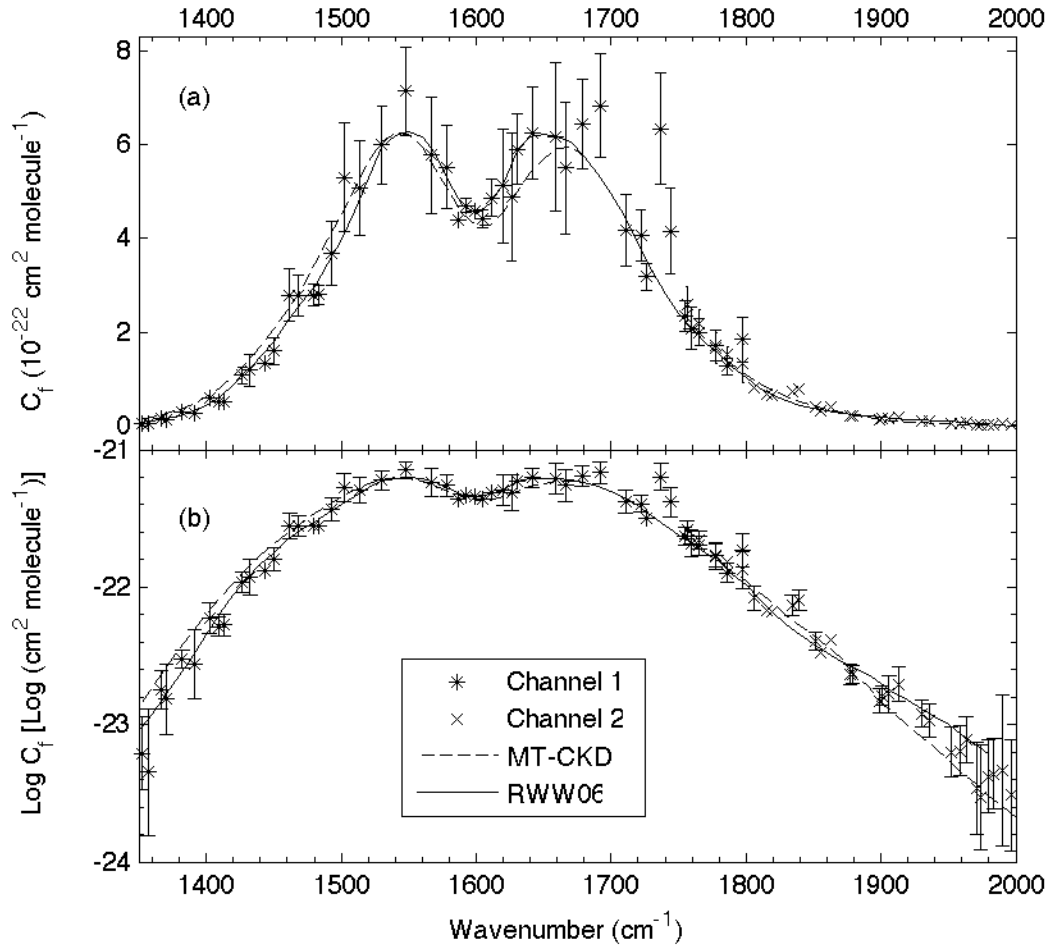


Fig. 5. (a) Final set of continuum coefficients retrieved in this work from Polar Atmospheric Infrared Radiance Interferometer (PAERI) measurements for the channel 1 and channel 2 detectors, and (b) the log of the continuum coefficients. Error bars are omitted where they are smaller than the symbol used. The MT-CKD continuum and the smoothed results of previous work (RWW06) are also shown.

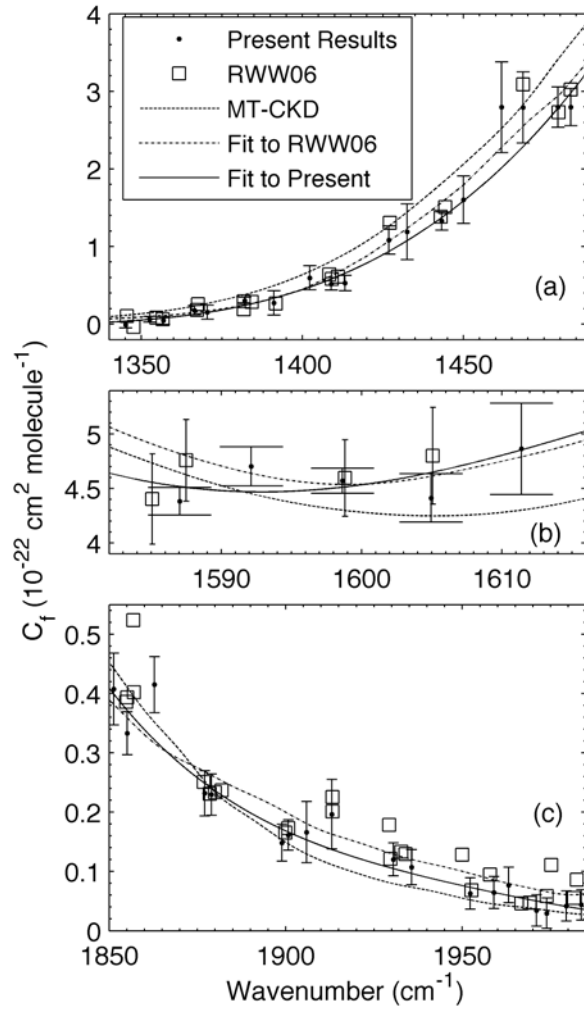


Fig. 6. Continuum coefficients retrieved from Polar Atmospheric Infrared Radiance Interferometer (PAERI) measurements in (a) the low-wavenumber wing of the  $\nu_2$  band, (b) the center, and (c) the high-wavenumber wing. The results of previous work (RWW06) and the MT-CKD continuum are shown.

Table 1. Continuum coefficients ( $C_f$ ) in the low wavenumber wing of the  $\nu_2$  band, from 1350 to 1490  $\text{cm}^{-1}$ , in continuum units, where  $1 \text{ CU} = 10^{-22} \text{ cm}^2 \text{ molecule}^{-1}$ . The columns are wavenumber ( $\nu$ ), the continuum model of Mlawer, Tobin, Clough, Kneizys, and Davies (MT-CKD), the polynomial fit to the results of Rowe et al. (2006; RWW06), the polynomial fit to the present results, and the uncertainty in the present results ( $\sigma$ ; one standard deviation), based on errors in the continuum coefficients.

$\nu$ ( $\text{cm}^{-1}$ )	$C_{f, \text{MT-CKD}}$ (CU)	$C_{f, \text{RWW06}}$ (CU)	$C_f$ (CU)	$\sigma$ (CU)
1350	0.13	0.09	0.05	0.04
1360	0.19	0.12	0.09	0.05
1370	0.26	0.17	0.15	0.08
1380	0.36	0.23	0.22	0.06
1390	0.48	0.32	0.32	0.1
1400	0.64	0.45	0.45	0.1
1410	0.83	0.64	0.60	0.08
1420	1.07	0.88	0.79	0.1
1430	1.36	1.16	1.01	0.3
1440	1.70	1.47	1.28	0.1
1450	2.06	1.80	1.59	0.3
1460	2.45	2.20	1.95	0.8
1470	2.90	2.60	2.35	0.5
1480	3.45	2.98	2.82	0.3
1490	3.97	3.45	3.34	0.5

Table 2. Continuum coefficients ( $C_f$ ) in the center of the  $\nu_2$  band, from 1350 to 1490  $\text{cm}^{-1}$ , in continuum units, where  $1 \text{ CU} = 10^{-22} \text{ cm}^2 \text{ molecule}^{-1}$ . The columns are wavenumber ( $\nu$ ), the continuum of Mlawer, Tobin, Clough, Kneizys, and Davies (MT-CKD), the polynomial fit to the results of Rowe et al. (2006; RWW06), the polynomial fit to the present results, and the uncertainty in the present results ( $\sigma$ ; one standard deviation), based on errors in the continuum coefficients.

$\nu$ ( $\text{cm}^{-1}$ )	$C_{f, \text{MT-CKD}}$ (CU)	$C_{f, \text{RWW06}}$ (CU)	$C_f$ (CU)	$\sigma$ (CU)
1590	4.52	4.71	4.48	0.1
1600	4.28	4.54	4.53	0.1
1610	4.28	4.75	4.80	0.4

Table 3. Continuum coefficients ( $C_f$ ) in the high wavenumber wing of the  $\nu_2$  band, from 1860 to 1970  $\text{cm}^{-1}$ , in continuum units, where  $1 \text{ CU} = 10^{-22} \text{ cm}^2 \text{ molecule}^{-1}$ . The columns are wavenumber ( $\nu$ ), the continuum of Mlawer, Tobin, Clough, Kneizys, and Davies (MT-CKD), the polynomial fit to the results of Rowe et al. (2006; RWW06), the polynomial fit to the present results, and the uncertainty in the present results ( $\sigma$ ; one standard deviation), based on errors in the continuum coefficients.

$\nu$ ( $\text{cm}^{-1}$ )	$C_{f, \text{MT-CKD}}$ (CU)	$C_{f, \text{RWW06}}$ (CU)	$C_f$ (CU)	$\sigma$ (CU)
1860	0.37	0.33	0.34	0.04
1870	0.30	0.29	0.28	0.04
1880	0.23	0.26	0.24	0.04
1890	0.19	0.23	0.20	0.04
1900	0.15	0.2	0.17	0.03
1910	0.12	0.17	0.14	0.03
1920	0.10	0.15	0.12	0.04
1930	0.08	0.13	0.11	0.03
1940	0.07	0.11	0.09	0.03
1950	0.06	0.10	0.07	0.03
1960	0.04	0.08	0.06	0.03
1970	0.04	0.07	0.05	0.03
1980	0.03	0.06	0.04	0.03